SCIENCE CHINA
Earth Sciences

• RESEARCH PAPER •

December 2013 Vol.56 No.12: 2116–2125
doi: 10.1007/s11430-013-4715-1

Rapid exhumation of the Tianshan Mountains since the early Miocene: Evidence from combined apatite fission track and (U-Th)/He thermochronology

LÜ HongHua[1,2*], CHANG Yuan[2], WANG Wei[2] & ZHOU ZuYi[2]

[1] *School of Resources and Environmental Science, East China Normal University, Shanghai 200241, China;*
[2] *State Key Laboratory of Marine Geology, Tongji University, Shanghai 200092, China*

Received September 14, 2012; accepted March 28, 2013; published online October 29, 2013

Combined apatite fission track (AFT) and (U-Th)/He (AHe) thermochronometries can be of great value for investigating the history of exhumation of orogenic belts. We evaluate the results of such a combined approach through the study on rock samples collected from the Baluntai section in the Tianshan Mountains, northwestern China. Our results show that AFT ages range from ~60 to 40 Ma and AHe ages span ~40–10 Ma. Based on the strict thermochronological constraints imposed by AHe ages, forward modeling of data derived from AFT analyses provides a well-constrained Cenozoic thermal history. The modeled results reveal a history of relatively slow exhumation during the early Cenozoic times followed by a significantly accelerated exhumation process since the early Miocene with the rate increasing from <30 m/Myr to >100 m/Myr, which is consistent with the inference from the exhumation rates calculated based on both AFT and AHe age data by age-closure temperature and mineral pair methods. Further accelerated exhumation since the late Miocene is recorded by an AHe age (~11 Ma) from the bottom of the Baluntai section. Together with the previous low-temperature thermochronological data from the other parts of the Tianshan Mountains, the rapid exhumation since the early Miocene is regarded as an important exhumation process likely prevailing within the whole range.

fission track, (U-Th)/He, exhumation, Cenozoic, the Tianshan Mountains

Citation: Lü H H, Chang Y, Wang W, et al. Rapid exhumation of the Tianshan Mountains since the early Miocene: Evidence from combined apatite fission track and (U-Th)/He thermochronology. Science China: Earth Sciences, 2013, 56: 2116−2125, doi: 10.1007/s11430-013-4715-1

The India-Asia collision during the early Cenozoic (Najman et al., 2001) is a very spectacular scene in the evolution history of the Earth. The resulted geological processes such as compressing, uplifting, thrusting and slipping from this collision have significantly impacted the tectonic and topographic patterns of northwestern China as well as the Central Asia (Zhang et al., 1996). In response to the collision, the Tianshan orogen has been tectonically reactivated and uplifted and intensely extended into both its northern and southern foreland basins (Avouac et al., 1993; Zhang et al., 1996; Deng et al., 2000). The history of uplift and exhumation of the Tianshan Mountains is thus crucial to understand tectonic deformation and mechanism of orogenic belts in the interior of Asia in relation to the India-Asia collision (Zhang et al., 1996).

Low-temperature thermochronometries, e.g., apatite and zircon fission track (AFT and ZFT), are potentially powerful tools for providing valuable information on the more recent geological history of orogenic belts, which is helpful to quantitatively study orogenic exhumation and regional erosion (e.g., Hendrix et al., 1994; Reiners et al., 2003; Reiners and Brandon, 2006). During the past few years, these two thermochronometries have been successfully used

*Corresponding author (email: hhlv@geo.ecnu.edu.cn)

to decipher the history of the Mesozoic and Cenozoic uplift and exhumation of the different areas within the Tianshan Mountains, such as the northern Tianshan Mountains and its foreland basin (e.g., Hendrix et al., 1994; Dumitru et al., 2001; Guo et al., 2005, 2006; Du and Wang, 2007; Zhang et al., 2007), Bogeda Mountain and Haerlike Mountain in the eastern Tianshan Mountains (e.g., Shen et al., 2006, 2008; Zhu et al., 2006; Wang et al., 2007; Li et al., 2008), the central Tianshan Mountains (e.g., Chen et al., 2006, 2008; Du and Wang, 2007), the southern Tianshan Mountains and its foreland basin (e.g., Sobel and Dumitru, 1997; Dumitru et al., 2001; Yang et al., 2003; Du and Wang, 2007; Du et al., 2007) and the southwestern Tian Shan foreland (e.g., Sobel and Dumitru, 1997; Dumitru et al., 2001; Zhang et al., 2009). These previous studies have largely promoted our understanding on the Mesozoic and Cenozoic tectonic evolution and exhumation of the Tianshan Mountains.

In the past decade, (U-Th)/He thermochronology has been greatly developed and have been successfully used in studies on orogenic exhumation, surface erosion and depositional process (e.g., Reiners et al., 2003; Zhou et al., 2003; Reiners and Brandon, 2006; Burbank et al., 2007). Compared with the other low-temperature thermochronometries, (U-Th)/He dating system has the lower closure temperature. For example, the closure temperature of apatite (U-Th)/He (AHe) is ~70°C (Farley, 2002), lower than the closure temperature of ~110°C in AFT dating system (Ketcham et al., 1999). Thus, (U-Th)/He thermochronometry can provide more information on changes in shallow-crust processes and has been thus used to probe into geomorphologic processes (e.g., House et al., 1998; Shuster et al., 2005) and reconstruct paleotopography (e.g., Reiners, 2007; Wang and Zhou, 2009). Furthermore, combined AFT and AHe thermochronological results may lead to new insights into upper crustal time-temperature paths and surface processes affecting annealing. Some studies (e.g., Bullen et al., 2001, 2003; Reiners et al., 2003; Zhou et al., 2003; Reiners and Brandon, 2006; Burbank et al., 2007) have shown the effectiveness of this approach in reconstructing the history of exhumation of orogenic belts. However, few studies use such a combined approach to constraining the history of exhumation of the Tianshan Mountains during the Cenozoic. Here we employ both AFT and AHe analyses on the samples taken from the Baluntai section in the Tianshan Mountains, northwestern China. The goals of this paper are (1) to reveal the exhumation process at the Baluntai area based on our low-temperature thermochronologic data, and (2) further to discuss the characteristics of the Cenozoic exhumation of the Tianshan Mountains, combined with the previous low-temperature thermochronologic results from the different areas of the range.

1 Regional geological setting

The Tianshan Mountains, stretching ~2500 km from east to west with the north-south width of ~250–350 km, is one of the largest and most active ranges in the Central Asia. Many previous studies (e.g., Windley et al., 1990; Avouac et al., 1993; Yin et al., 1998) show that the ancestral Tianshan Mountains was formed after experiencing several collisions and amalgamations of blocks during the Late Devonian-Early Carboniferous and Late Carboniferous-Early Permian, along with the formation of a suit of east-west trending strike-slip and thrust faults (Figure 1). The subsequent Mesozoic deformation of the Tianshan orogen is characterized by the relative tectonic stability (pediplanation) during the Triassic-Late Jurassic, followed by the active tectonic deformation during the Late Jurassic-Early Cretaceous. During the latest Mesozoic and Paleogene, the relative tectonic stability prevailing in the Tianshan orogen resulted in the beveling of topography (Zhang and Wu, 1985; Allen et al., 1991; Bullen et al., 2003). Different authors have proposed that the Tianshan Mountains has existed as a positive physiographical feature separating the Junggar Basin to the north from the Tarim Basin to the south throughout the Mesozoic times (Hendrix et al., 1992). In response to the India-Asia collision during Early Cenozoic (Najman et al., 2001), the Tianshan orogen has been tectonically reactivated and uplifted and intensely extended into its foreland basins (Zhang et al., 1996; Shu et al., 2003). As a result, both the northern and southern Tian Shan foreland depressions (such as the Urumqi Depression, Kuqa Depression and Kashi Depression) have developed several belts of fault-related folds (Deng et al., 2000) (Figure 1).

Our work is focused on the Baluntai area of the Tianshan Mountains, Xinjiang, northwestern China (Figures 1 and 2), where the exposed lithological stratigraphy mainly comprises Proterozoic schist and Carboniferous conglomerate and sandy conglomerate as well as Variscan intrusive rock (Figure 2). As for the Mesozoic and Cenozoic, only the Triassic and Quaternary are exposed in local areas (Figure 2). Tectonically, the geological boundary between the central and southern Tianshan orogen lies near Uwamen in the Baluntai area (Ma et al., 2006). Some previous AFT analyses on rock samples from the Ulastai-Baluntai segment of the Urumqi-Kurla Road (UK Road) (Ma et al., 2006; Du and Wang, 2007) show a single thermal history of the intrusive rock in the Baluntai area.

2 Samples and analytical methods

The sampled Baluntai section is located in a valley ~2.5 km east of Baluntai Village of Baluntai Town in Hejing County, Xinjiang (42°41′N, 86°20′E) (Figure 2). The horizontal outcrop width of the Baluntai section approaches ~2 km and the vertical height is ~680 m (Figure 2). All the samples were taken from fresh bedrock outcrops of Variscan granite series with the vertical sampling interval of ~100–150 m. Portable GPS was used to determine the location and eleva-

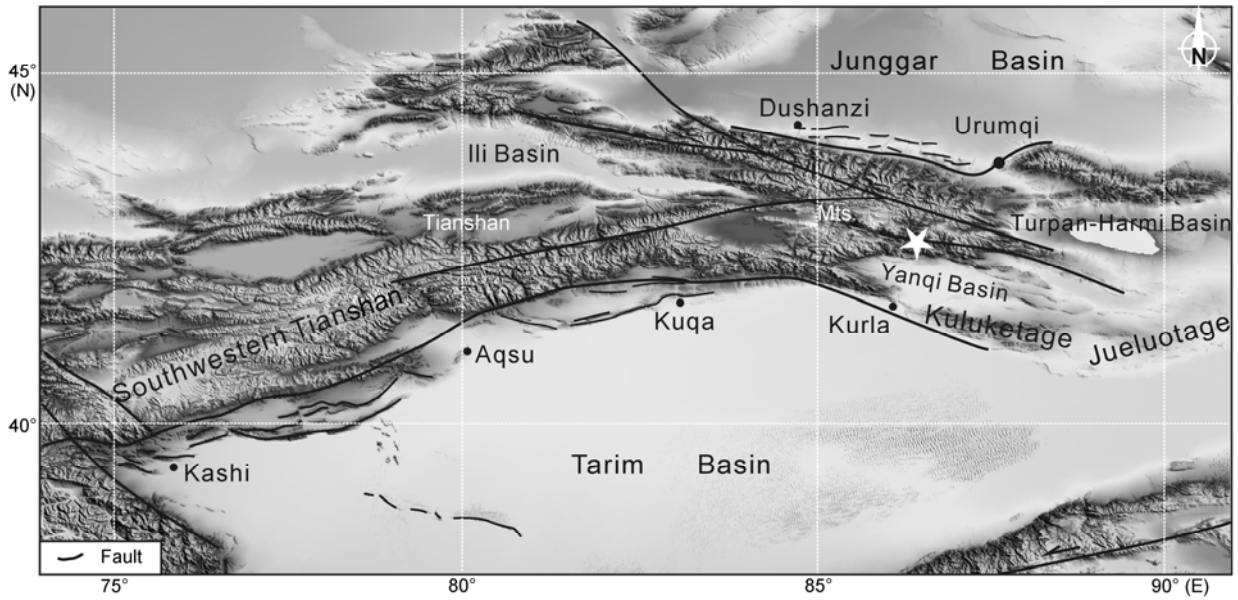

Figure 1 Digital elevation model (DEM) map showing topography and tectonics (Du and Wang, 2007; Gao et al., 2009; Fu et al., 2010) of the Tianshan Mountains and its surrounding area with a star indicating the location of the sampled Baluntai section.

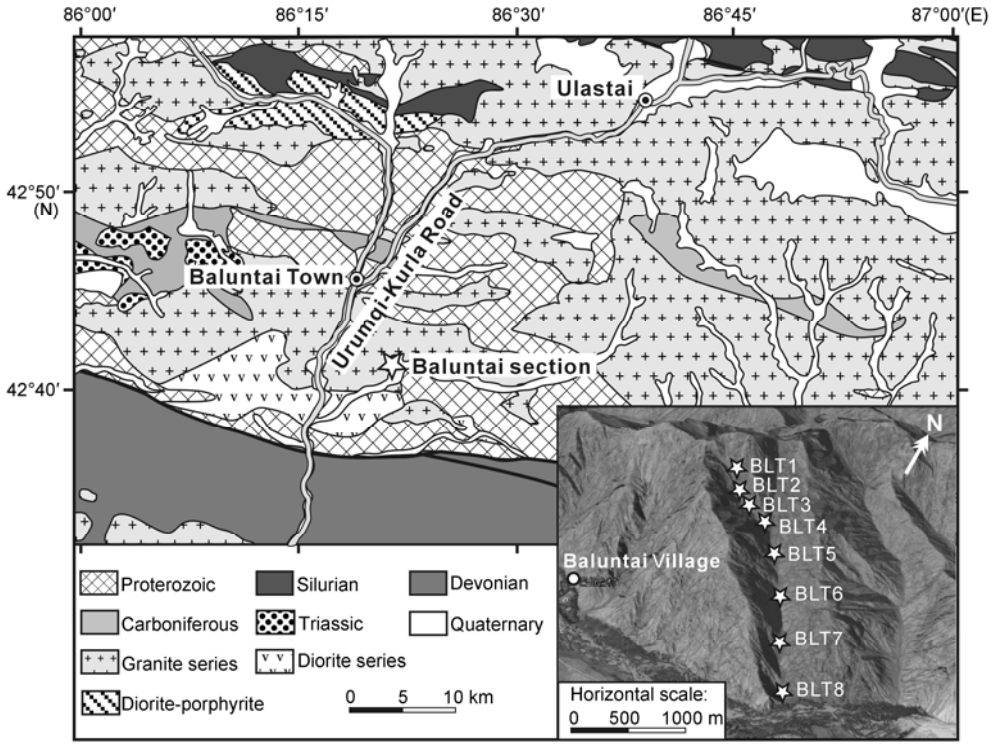

Figure 2 Geological map of the Baluntai area (based on 1∶200000 Baluntai and Yanqi geological maps) and inserted Google Earth image showing the sampled section and the sampling sites with open stars.

tion of each sample (see Table 1 for the detailed sampling information). The apatite crystals were separated from ~3–4 kg rock samples using standard magnetic and heavy liquid techniques. Approximately 500 apatite crystals were picked per sample. The selected apatite grains were then subjected to the following fission-track (FT) and (U-Th)/He thermochronological analyses.

The external detector (ED) method was used to perform AFT analysis. The analytical procedure for AFT analysis was completed in the Fission Track Laboratory of the State Key Laboratory of Marine Geology, Tongji University, Shanghai. Selected apatite grains were first embedded in

epoxy resin, polished to expose the internal surfaces of the crystals, and etched in 5.5 mol/L HNO_3 at 21±1 °C for 20±1 s (donelick, 1993) to reveal ^{238}U spontaneous fission tracks. The etching temperature was controlled with a thermostatic water bath. The exposed internal surfaces of the apatite crystals were then covered with low-uranium muscovite external detectors. The crystals with external detectors were packed together with the standard dosimetry glass of IRMM-540 (de Corte et al., 1998; Xu et al., 2005) and the standard apatite sample of Fish Canyon Tuff (FCT) (Hurford and Hammerschmidt, 1985), and then irradiated by using a thermal neutron fluence of 3.2E+15 in Laboratorio Energia Nucleare Applicata (LENA), Università degli Studi di Pavia, Italy. Induced tracks in muscovite external detectors were revealed by etching in 40% HF at room temperature for 40 min (Xu et al., 2005). Fission tracks counting and track length and D_{par} (Ketcham et al., 1999) measurements were done under the Autoscan Fission-track Dating System. The apatite crystals were dated by using the Zeta (ζ) calibration method (Hurford and Green, 1983) with the zeta value of 236.7±14.8 in this study. The AFT analytical data are listed in Table 2 and the ages are given with an error of ±1σ. All the lab work for AHe analysis was completed in the Laboratory for (U-Th)/He analysis, University of Arizona, USA. The analytical procedure is after that of Reiners and Nicolescu (2006). In this study, two apatite crystals selected from each sample were subjected to the AHe analysis. The AHe analytical data are listed in Table 3 and the ages are given with an error of ±1σ. The sample age was calculated as the arithmetic mean of two single grain ages.

In order to further understand the thermal history of the sampled Baluntai bedrock, the time-temperature history for samples with measured confined track lengths was modeled based on the AFT data using the HeFTy modeling software of Ketcham (2009) with the multi-kinetic annealing model of Ketcham et al. (2007) as well as Monte Carlo method (Ketcham, 2009). D_{par} (Ketcham et al., 1999) was used as the thermal kinetic parameter. The estimated initial track length L_o was calculated as L_o=0.283+15.63×D_{par} (Carlson et al., 1999) and Kolmogorov-Smirnov Test was used as the optimal length fitting equation. In each case, 10000 models were tested and only the best-fit curve was taken into account. When modeling, the temperature constraint was specified with local tectonic background and AHe ages, and the partial retention zone of AHe is 55–80°C (Farley, 2000). Length and age GOFs (goodness of fitting) are used to evaluate the fitting degree between modeled and measured results of fission track length and age, respectively. When

Table 1 Information on apatite fission-track samples of the Baluntai section

Sample No.	Sample elevation (m)	Sample location		Dating method	Thermochronological constraints on AFT thermal history modeling
		Latitude (N)	Longitude (E)		
BLT1	2480	42°41′7.3″	86°19′55″	AFT	–
BLT2	2386	42°41′5.8″	86°20′1.2″	AFT and AHe	38.67±0.7 Ma (AHe, this study)
BLT3	2251	42°41′4.8″	86°20′7.3″	AFT	–
BLT4	2147	42°41′5.8″	86°20′14.9″	AFT and AHe	31.14±0.56 Ma (AHe, this study)
BLT5	2054	42°41′4.4″	86°20′26.6″	no	–
BLT6	1956	42°40′58.8″	86°20′42.7″	AFT	–
BLT7	1862	42°40′53.7″	86°20′58.4″	AHe	–
BLT8	1796	42°40′47.1″	86°21′12.2″	AFT and AHe	–

Table 2 Apatite fission track dating data of the samples from the Baluntai section[a)]

Sample No.	N_c	Spontaneous track		Induced track		Standard dosimetry glass		$P(\chi^2)$ (%)	Age ±1σ (Ma)	Confined track			D_{par} (μm)
		ρ_s (×10^6 track/cm^2)	N_s	ρ_i (×10^6 track/cm^2)	N_i	ρ_d (×10^5 track/cm^2)	N_d			N_l	L_s±1σ (μm)	SD (μm)	
BLT1	22	1.607	440	0.898	246	2.99506	5990	19.2	63.1±6.4	–	–	–	–
BLT2	46	0.96	957	0.366	365	2.99141	5983	22.1	92.2±8.2	30	12.51±1.33	1.83	1.60
BLT3	11	0.446	154	0.24	83	2.98758	5975	94.4	65.3±9.8	–	–	–	–
BLT4	46	1.27	2317	0.745	1359	2.98355	5967	4.03	59.9±4.3	103	13.37±1.23	1.73	1.89
BLT6	29	1.121	699	0.911	568	2.97511	5950	<0.1	43.2±3.7	–	–	–	–
BLT8	37	0.587	769	0.321	421	2.97128	5943	11.5	63.9±5.6	–	–	–	–

a) Abbreviations are: N_c, number of apatite crystals analyzed per sample; ρ_s, spontaneous track density in analyzed apatite crystals; N_s, number of spontaneous tracks counted; ρ_i, induced track density in external detector for analyzed crystals; N_i, number of induced tracks counted; ρ_d, induced track density in an external detector adjacent to dosimetry glass; N_d, number of tracks counted in determining ρ_d; $P(\chi^2)$, chi-square probability; N_l, number of measured confined track lengths; SD, standard deviation of confined track length. D_{par} is the average of all the measured D_{par} values for each sample. IRMM-540 is used as the standard dosimetry glass (U=13.9±0.5 mg/kg, $^{235}U/^{238}U$=0.007277) (de Corte et al., 1998) and Fish Canyon Tuff (FCT) as the standard sample with the age of 27.8±0.7 Ma (Hurford and Hammerschmidt, 1985). AFT age = $\lambda_\alpha^{-1}\ln[1+\lambda_\alpha(\rho_s/\rho_i)\rho_d G\zeta]$, where λ_a=1.55125×10^{-10} a^{-1}, G=0.5 and ζ=236.7±14.8.

Table 3 Apatite (U-Th)/He dating data of the samples from the Baluntai section[a)]

Sample No.	Grain	Weight (μg)	MWAR (μm)	U (ppm)	Th (ppm)	^{4}He (nmol/g)	F_t	Corrected grain age ±1σ (Ma)	Sample age ±1σ (Ma)
BLT2	A	7.85	71.25	9.92	2.12	2.06	0.81	44.89±0.93	38.67±0.70
	B	6.76	69.75	5.04	83.34	3.44	0.79	32.44±0.46	
BLT4	A	15.43	94.5	36.96	3.73	5.39	0.86	30.75±0.56	31.14±0.56
	B	34.53	104.25	27.8	2.02	4.24	0.88	31.52±0.56	
BLT7	A	21.52	112	17.32	0.36	3.64	0.87	44.0±0.83	44.0±0.83
	B	0.41	25.25	45.53	5.89	14.5	0.49	(115.78±2.62)	
BLT8	A	2.76	47.75	15.45	4.87	0.72	0.73	10.92±0.31	10.92±0.31
	B	1.09	43.25	357.61	873.49	145.45	0.67	(70.56±0.97)	

a) MWAR is mass-weighted average radius. F_t is fraction of total alpha particles retained. The sample age is calculated as the average of two single grain ages. The single grain ages of BLT7-B and BLT8-B (shown by parentheses) were not used to calculate the sample AHe ages. See the text for the interpretation.

length and age GOFs are >5%, the modeled time-temperature curves are regarded as acceptable. When these two GOFs are >50%, the modeled curves are of good quality.

3 Results

3.1 Fission track length distribution and thermal modeling

The character of the thermal history can be reflected by the track length distribution. In general, the initial length of apatite fission track is 16.3±0.9 μm (Gleadow et al., 1986). Fission tracks will be annealed and track length will be shortened when temperature becomes higher than the closure temperature of the dating system. Thus, fission track length distribution can be used to characterize the thermal history experienced by some specified rock sample, and different track length compositions can represent different stages of the whole thermal history that this sample has experienced. Except for temperature, the factors affecting the annealing of fission tracks include chemical composition of mineral (Green et al., 1985), track angle to the crystallographic *c*-axis (Donelick and Miller, 1991) and D_{par} (Donelick et al., 1999; Ketcham et al., 1999). In this study, the mean confined track lengths of samples BLT2 and BLT4 are 12.51 and 13.37 μm, respectively (Table 2). Both the track length distributions are characteristically unimodal (Figure 3), probably signaling that the sampled Baluntai bedrock could have experienced a single thermal history (Gleadow et al., 1986). The peak values of ~13–15 μm in both these two track length distributions are regarded as indicative of rapid postorogenic exhumation. The modeled thermal histories (Figure 3) based on the AFT data are consistent with this inference.

In this study, both length and age GOFs for the analyzed samples are >80% (Figure 3), and thus the modeled results are of high quality. Generally, the number of measured confined track lengths for thermal modeling should exceed 40 and high reliability demands more than 100 measured track lengths. To sample BLT4, the number of confined track lengths is 103, much more than 30 confined track lengths of BLT2. Thus, the modeled history of BLT4 should be more reliable than the models of BLT2 due to more confined track lengths. The modeled results show that samples BLT2 and BLT4 have similar thermal history curves, suggesting that these two samples experienced a similar thermal history during the Cenozoic (Figure 3): relatively slow cooling during Paleogene followed by subsequent rapid cooling since Miocene. However, it appears that BLT4 might have experienced a relatively rapid cooling process during Paleogene than that of BLT2 according to the modeled thermal history curves (Figure 3).

3.2 Exhumation rate

Generally, exhumation is referred to as displacement of rock with respect to the surface. The rate of exhumation is simply the rate of removal of overburden caused by surface erosion and/or tectonic processes, which can be extracted from thermochronological data. We calculate exhumation rates on the basis of the modeled thermal history and AFT and AHe age data (Tables 2 and 3). Here AHe ages of grains BLT7-B and BLT8-B are not used for the exhumation rate analysis due to the following reasons: (1) The 25.25-μm mass-weighted average radius of apatite grain BLT7-B is smaller than the general measurement demand of 30 μm, which likely caused its abnormal AHe age of ~116 Ma (older than the AFT ages of the samples from the section). (2) Compared with the other apatite grains, the concentrations of U, Th and He in the grain BLT8-B are extremely high. This may be attributed to the existence of mineral inclusion (e.g., zircon inclusion) containing high radioactive elements (Vermeesch et al., 2007), thus yielding an abnormal AHe age of ~71 Ma. However, the two comparable single grain ages of samples BLT2 and BLT4 (Table 3) indicate that the lab treatments and measurements are reliable in this study.

The basic methods of extracting the exhumation rate from low-temperature thermochronological data include thermal modeling, age-closure temperature, mineral pair

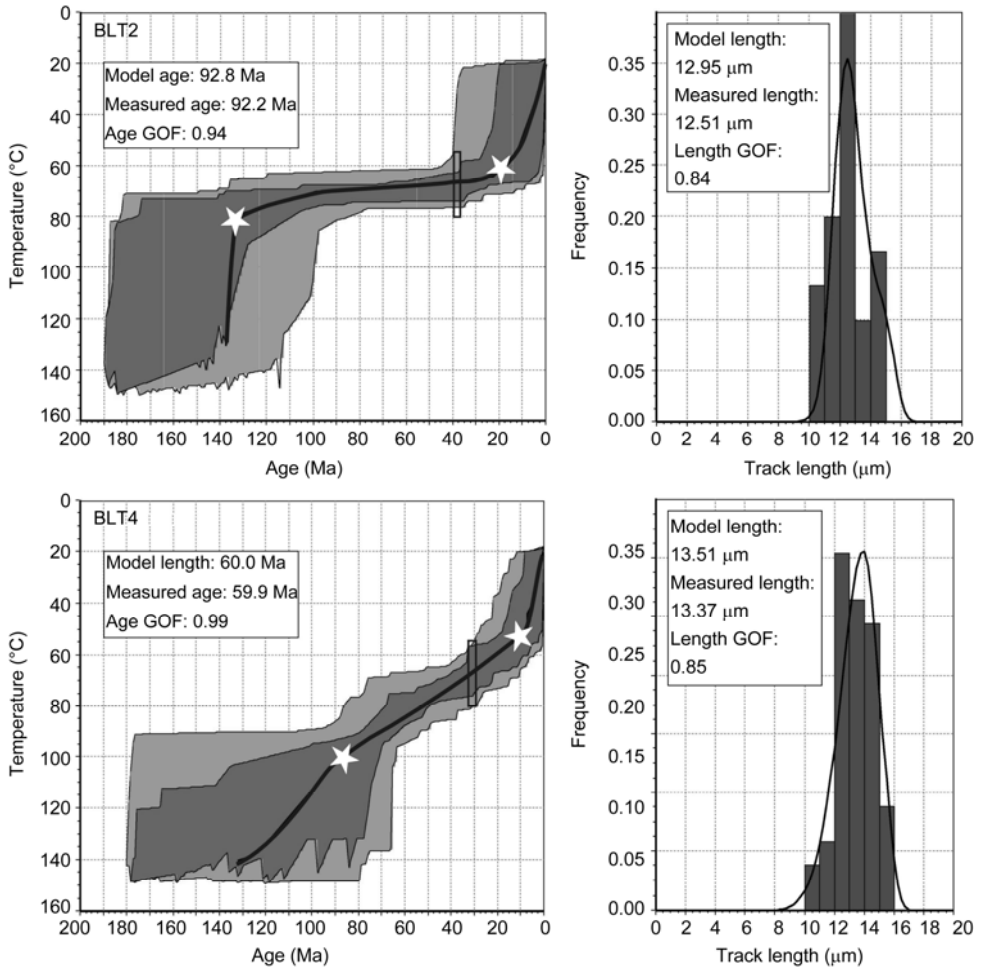

Figure 3 Fission track length distribution and modeled thermal history of the apatite samples from the Baluntai section in the southern Tianshan Mountains, northwestern China. Grayish zone represents acceptable modeled time-temperature curves (GOF >5%) and dark gray zone represents the modeled results of high quality (GOF >50%). Heavy line represents the best fitting result. Rectangles show the chronological constraint by AHe age and stars indicate the time when the rate of cooling significantly changes.

and age-elevation relationship methods (Ding et al., 2007; Chang and Zhou, 2010). Thermal modeling method is to use the time span of cooling and the corresponding cooling temperature to calculate exhumation rates of different cooling stages of the thermal history based on an assumed paleogeothermal gradient. As for age-closure temperature method, the rate can be calculated on the basis of the cooling age and the closure temperature of the dating system as well as the assumed paleogeothermal gradient. Mineral pair method converts the age difference recorded by two thermochronometries with different closure temperatures (e.g., AFT and AHe) to the rate of exhumation. Age-elevation relationship method is to use the correlation between the cooling ages and elevation data of samples collected from some vertical profile to extract the regional exhumation rate. This method avoids the presupposition of the paleogeothermal gradient in comparison with the other methods (Chang and Zhou, 2010). It is clear that these above methods focus on different time spans due to using different thermochronological data. Here we do not employ age-elevation relationship method when considering the limit sampling height of the Baluntai section (<700 m) as well as the insignificant relationship between age and elevation data of the section. Guo et al. (2006) have recently reported an AFT thermochronological study on the samples collected along the Houxia-Shenglidaban segment of the UK Road across the Tianshan Mountains. Their results show that a likely positive relationship appears to exist between AFT ages and elevations of the samples. However, the horizontal outcrop width of Guo et al.'s section (2006) is obviously larger than the critical sampling width of ~5 km for an AFT age-elevation profile yielding an acceptable rate of exhumation with <15% error (Chang et al., 2010). Thus age-elevation relationship method is also not suitable for their section. Here we use thermal modeling, age-closure temperature and mineral pair methods to calculate the exhumation rate. We assume that the closure temperatures of AHe and AFT dating systems are 70 (Farley, 2002) and 110°C (Ketcham et al., 1999), respectively, and that the paleogeothermal gradient is 22°C/km (Hendrix et al., 1994). The

present surface temperature is 10°C. The results are listed in Table 4.

The exhumation rates shown in Table 4 display some notable characters of the Cenozoic exhumation processes in the Baluntai area in the southern Tianshan Mountains. The modeled thermal history curves (Figure 3) indicates a significantly accelerated exhumation process since the early Miocene. Correspondingly, the rates of exhumation extracted from the modeled results show a >300% increase from <~30 m/Myr to >100 m/Myr (Table 4).

Based on age-closure temperature method, the exhumation rates constrained by AFT and AHe ages are ~50–100 m/Myr and ~60–250 m/Myr, respectively (Table 4). Given that the cooling age of a mineral should record the time at which it became cool enough to retain the daughter products or the fission tracks produced by the decay of radioactive isotopes, the exhumation rate calculated by age-closure temperature method is thus a mean rate over the time when a rock cooled below the specific blocking temperature. Furthermore, this calculated rate can be regarded as an overall reflection of both the slow and rapid cooling stages during the Cenozoic revealed by thermal modeling in this study. Correspondingly, the value of the calculated exhumation rate should be between the rates extracted from these two cooling stages by thermal modeling method. For example, to samples BLT2 and BLT4, the exhumation rates constrained by AFT and AHe ages are ~49–71 and ~76–88 m/Myr, respectively. Both of them are within the limit of rates of ~10 to 160 m/Myr extracted from the modeled thermal history (Table 4). In addition, to samples BLT2, BLT4 and BLT8, the exhumation rates constrained by AHe ages are obviously larger than that calculated on the basis of AFT ages (Table 4). This suggests that these samples could have recorded an accelerated exhumation process during the late Cenozoic, given the fact that (U-Th)/He thermochronometry records a more recent history of exhumation and cooling due to the lower blocking temperature in comparison to FT thermochronological system. The magnitude of increase in exhumation rate is determined to >15% (Table 4). Based on AHe age of sample BLT8, the magnitude since ~11 Ma might even be >250%. All these rates of exhumation shown in Table 4 are regarded to likely reveal a progressively accelerated exhumation process during the late Cenozoic in the present study area.

Using AFT and AHe ages, mineral pair method constrains the exhumation rates of ~30–65 m/Myr (Table 4), smaller than the rates of ~60–250 m/Myr calculated on the basis of AHe age-closure temperature method (Table 4). Because fission-track and (U-Th)/He ages of a mineral record different time spans due to various blocking temperatures, this suggests that the exhumation process during Paleocene-latest Eocene might be relatively slow in the Baluntai area, and that the exhumation began to accelerate since the latest Eocene. During Miocene, the exhumation was significantly accelerated and the rate might be >~200 m/Myr.

4 Discussion

As shown above, the exhumation rates extracted from AFT and AHe data indicate a similar exhumation history during the Cenozoic in the Baluntai area in the Tianshan Mountains, which is characterized by a rapid exhumation process since the early Miocene with the rate of >100 m/Myr. The exhumation rate since ~11 Ma might even be larger than ~200 m/Myr. Du and Wang (2007) and Ma et al. (2006) have performed apatite fission-track thermochronological studies on rock samples from the Ulastai-Baluntai segment of the UK Road. Ma et al. (2006) have proposed that the Cenozoic exhumation history is characterized by Paleocene and Miocene rapid exhumation processes. The modeled thermal results of Du and Wang (2007) show a different Cenozoic exhumation history from that presented in this study: the Early Eocene-Miocene rapid exhumation followed by the subsequent slow exhumation process. Such a

Table 4 Exhumation rates constrained by thermal modeling, age-closure temperature and mineral pair methods in the Baluntai section (m/Myr)[a)]

Sample No.	Thermal modeling method		Age-closure temperature method				Mineral pair method (AFT/AHe)
			AFT		AHe		
	Exhumation rate during slow exhumation stage (time span)	Exhumation rate during rapid exhumation stage (time span)	Age (Ma)	Exhumation rate	Age (Ma)	Exhumation rate	Exhumation rate (time span)
BLT1	–	–	63.1	72	–	–	–
BLT2	7.9 (~135–20 Ma)	102.3 (since ~20 Ma)	92.2	49.3	38.67	70.5	34 (92.2–38.7 Ma)
BLT3	–	–	65.3	69.6	–	–	–
BLT4	30.3 (~85–10 Ma)	159.1 (since ~10 Ma)	59.9	75.9	31.14	87.6	63.2 (59.9–31.1 Ma)
BLT6	–	–	43.2	105.2	–	–	–
BLT7	–	–	–	–	44	62	–
BLT8	–	–	63.9	71.1	10.92	249.8	34.3 (63.9–10.9 Ma)

a) The thermochronological data used in thermal modeling method are from the modeled results shown in Figure 3. The rate of exhumation based on age-closure temperature method is a mean rate over the cooling age. The rate of exhumation based on mineral pair method is a mean rate during the period constrained by the AFT and AHe ages.

difference is attributed to the different analytical methods. Our integrated AFT and AHe thermochronolgical analyses provide improved thermochronological constraints on the modeled thermal histories in comparison to those previous studies.

Geomorphologically and tectonically, the Tianshan Mountains can be divided into the eastern Tianshan Mountains, northern Tianshan Mountains, central Tianshan Mountains, southern Tianshan Mountains and southwestern Tianshan Mountains (Li et al., 2006). The Baluntai area is located within the central Tianshan Mountains, where the history of exhumation during the Cenozoic is characterized by the rapid exhumation since the early Miocene revealed by our thermochronological data. This exhumation process is consistent with the other AFT thermochronological results from the other parts within the Tianshan Mountains. In the Bogda Mountains of the eastern Tianshan Mountains, the AFT thermochronological data reveal a rapid exhumation event that occurred at ~25 Ma (Guo et al., 2005, 2006; Shen et al., 2008) followed by the ~10±2-Ma rapid exhumation (Zhu et al., 2006; Wang et al., 2007; Li et al., 2008). The ~25-Ma rapid exhumation process is also revealed in the Balikun Mountains to the east of the Bogda Mountains (Li et al., 2008). In the north piedmont of the Tianshan Mountains, the AFT thermochronological analyses from the Manas section (Hendrix et al., 1994; Du and Wang, 2007) and Toutunhe section (Du and Wang, 2007) indicate that the thrusting and extension of the Tianshan orogen into the southern Junggar Basin at ~25 Ma caused the folding and exhumation of the Mesozoic and Cenozoic sequences in the piedmont depression zones, which signaling the synchronous uplift and north-south convergence of the Tianshan orogen. In this piedmont, the persistent extension of the range into its foreland basin during the Cenozoic caused acceleration in exhumation at ~10 Ma (Zhang et al., 2007). In the Ilianhabirga Mountains and Boluoklu Mountains of the northern Tianshan Mountains, a prevailed rapid exhumation process was dated at ~25 Ma (Guo et al., 2005; Du and Wang, 2007; Shen et al., 2008), although the main exhumation during the Cenozoic commenced since the middle Eocene (Du and Wang, 2007; Shen et al., 2008). In the Chahanwusu Mountains and Keguqin Mountains of the central Tianshan Mountains, thermal modeling constrains the rapid exhumation at ~24 Ma (Chen et al., 2006, 2008), when differentiate tectonic evolution caused the co-existing range uplift and basin depression in this region. In the southern piedmont of the Tianshan Mountains and the southwestern Tian Shan foreland basin, low-temperature thermochronologial studies reveal the rapid exhumation during the latest Oligocene-middle Miocene (Sobel and Dumitru, 1997; Dumitru et al., 2001; Yang et al., 2003; Du and Wang, 2007; Zhang et al., 2009) in response to thrusting and extension of the range into the northern Tarim Basin (Zhang et al., 1996; Deng et al., 2000). All these above low-temperature thermochronological data show the rapid exhumation process since the early Miocene prevailing within the whole Tianshan Mountains.

The Cenozoic terrigenous sequences deposited in both northern and southern Tian Shan foreland basins have recorded the rapid exhumation of the range since the early Miocene. The lithofacies transition in the Kuqa River section in the southern Tian Shan foreland indicates the commencement of the southward extension of the Tianshan orogen and the resultant deformation of the piedmont thrust-fold belts at ~21–24 Ma (Yin et al., 1998), synchronous with the Latest Oligocene-Middle Miocene rapid exhumation process (Dumitru et al., 2001; Yang et al., 2003; Du and Wang, 2007). In the Junggar Basin, Métivier and Gaudemer (1997) found that the sediment-accumulation rate in the Cenozoic terrigenous succession significantly accelerated at ~16 Ma. This acceleration in sedimentation rate was causally linked with the Latest Oligocene-Middle Miocene rapid exhumation as a result of tectonic uplift of the Tianshan Mountains (Métivier and Gaudemer, 1997).

Combined AFT and AHe thermochronometries can improve thermal modeling and provide more valuable information on the history of postorogenic exhumation and evolution (e.g., Bullen et al., 2001, 2003; Reiners et al., 2003; Zhou et al., 2003; Reiners and Brandon, 2006; Burbank et al., 2007). Here we tentatively study the Cenozoic exhumation process in the Baluntai area in the southern Tianshan Mountains using such a combined approach. However, the exhumation process at any single location within the Tianshan Mountains may only indicate local tectonic influences, rather than range-wide changes. Future combined AFT and AHe thermochronological analyses should focus on the different areas of the Tianshan Mountains in order to better constrain the Cenozoic exhumation history of the range.

5 Conclusions

Our integrated AFT and AHe thermochronological analyses provide new data for deciphering the Cenozoic exhumation history of rock samples from the Baluntai section in the southern Tianshan Mountains, northwestern China. All the samples yielded AFT ages spanning ~60–40 Ma and AHe ages ranging from ~40 to 10 Ma. The time-temperature history curves based on AFT data indicate the rapid exhumation process since the early Miocene in the Baluntai area. This inference is consistent with the interpretation from the rates of exhumation based on thermal modeling, age-closure temperature and mineral pair methods. During the late Miocene, the exhumation rate was likely larger than ~200 m/Myr. Together with the previous low-temperature thermochronological data from the other areas of the Tianshan Mountains, we propose that the rapid exhumation since the early Miocene might have prevailed within the Tianshan Mountains. The sedimentary records from the intermontane

and foreland basins of the Tianshan Mountains provide further supports for this rapid exhumation process. Future combined AFT and AHe thermochronological studies should focus on the different areas of the Tianshan Mountains in order to better constrain the history of the Cenozoic exhumation of the range.

We are grateful to the referees for their thoughtful comments and suggestions. We thank Professor Reiners P. W. at University of Arizona for his help in (U-Th)/He analyses and Professor Xu Changhai at Tongji University for his assistance in the apatite fission track analyses. Wang Xucheng, Jiao Ruohong and Wang Chao are appreciated for their assistance in the lab. Lu Honghua gives special appreciation to Professor Li Youli at Peking University and Professor Zheng Xiangmin at East China Normal University for their help. This study was financially supported by National Natural Science Foundation of China (Grant No. 41001002) and China Postdoctoral Science Special Foundation (Grant No. 201003277).

Allen M B, Windley B F, Zhang C, et al. 1991. Basin evolution within and adjacent to the Tien Shan Range, NW China. J Geol Soc, 148: 369–378

Avouac J-P, Tapponnier P, Bai M, et al. 1993. Active thrusting and folding along the northern Tien Shan and late Cenozoic rotation of the Tarim relative to Dzungaria and Kazakhstan. J Geophys Res, 98: 6755–6804

Bullen M E, Burbank D W, Garver J, et al. 2001. Late Cenozoic tectonic evolution of the northwestern Tien Shan: New age estimates for the initiation of mountain building. Geol Soc Am Bull, 113: 1544–1559

Bullen M E, Burbank D W, Garver J. 2003. Building the northern Tien Shan: Integrated thermal, structural, and topographic constraints. J Geol, 111: 149–165

Burbank D W, Brewer I D, Sobel E R, et al. 2007. Single-crystal dating and the detrital record of orogenesis. In: Nichols G, Williams E, Paola C, eds. Sedimentary Processes, Environments and Basin: A Tribute to Peter Friend. Special Publication of the International Association of Sedimentologists (38). Hoboken: John Wiley and Sons. 253–281

Carlson W D, Donelick R A, Ketcham R A. 1999. Variability of apatite fission-track annealing kinetics I: Experimental results. Am Mineral, 84: 1213–1223

Chang Y, Zhou Z Y. 2010. Basic methods to inverse exhumation rates using low-temperature thermochronological data (in Chinese). Sci Tech Rev, 28: 86–94

Chang Y, Wang W, Zhou Z Y. 2010. Age-elevation relationship method limited by the topographic relief over the sampling transect (in Chinese). China J Geophys, 53: 1868–1874

Chen Z L, Wan J L, Liu J, et al. 2006. Multi-stage uplift and exhumation of the west Tianshan Mountain: Evidence from the apatite fission-track dating (in Chinese). Acta Geosci Sin, 27: 97–106

Chen Z L, Li L, Liu J, et al. 2008. Preliminary study on the uplifting-exhumation process of the western Tianshan range, northwestern China (in Chinese). Acta Petrol Sin, 24: 625–636

Deng Q D, Feng X Y, Zhang P Z, et al. 2000. Active Tectonics of the Tianshan Mountains (in Chinese). Beijing: Seismological Press. 339

De Corte F, Bellemans F, van den Haute P, et al. 1998. A new U doped glass certified by the European commission for the calibration of fission-track dating. In: van den Haute P, de Corte F, eds. Advances in Fission-track Geochronology. Dordrecht: Kluwer Academic Publishers. 67–78

Ding R X, Zhou Z Y, Wang W. 2007. Modeling exhumation rates of orogenic belts with low-temperature thermochronological data (in Chinese). Adv Earth Sci, 22: 447–455

Donelick R A, Miller D S. 1991. Enhanced tint fission track densities in low spontaneous track density apatites using ^{252}Cf-derived fission fragment tracks: A model and experimental observations. Nucl Tracks Radiat Meas, 18: 301–307

Donelick R A. 1993. Method of fission track analysis utilizing bulk chemical etching of apatite. United States Patent, Number 5267274. 1993-11-30

Donelick R A, Ketcham R A, Carlson W D. 1999. Variability of apatite fission track annealing kinetics II: Crystallographic orientation effects. Am Mineral, 84: 1224–1234

Du Z L, Wang Q C. 2007. Mesozoic and Cenozoic uplift history of the Tianshan region: Insight from apatite fission track (in Chinese). Acta Geol Sin, 81: 1081–1101

Du Z L, Wang Q C, Zhou X H. 2007. Mesozoic and Cenozoic uplift history of the Range-Basin system at Kuche from fission track analysis (in Chinese). Petrol Mineral, 26: 399–408

Dumitru T A, Zhou D, Chang E Z, et al. 2001. Uplift, exhumation, and deformation in the Chinese Tian Shan. In: Hendrix M S, Davis G A, eds. Paleozoic and Mesozoic Tectonic Evolution of Central and Eastern Asia: From Continental Assembly to Intracontinental Deformation. Geol Soc Am Memoir, (194): 71–99

Farley K A. 2000. Helium diffusion from apatite: General behavior as illustrated by Durango fluorapatite. J Geophys Res, 105: 2903–2914

Farley K A. 2002. (U-Th)/He dating: Techniques, calibrations, and applications. Rev Mineral Geochem, 47: 819–844

Fu B H, Ninomiya Y, Guo J M. 2010. Slip partitioning in the northeast Pamir-Tian Shan convergence zone. Tectonophysics, 483: 344–364

Gao J, Qian Q, Long L L, et al. 2009. Accretionary orogenic process of Western Tianshan, China (in Chinese). Geol Bull Chin, 28: 1804–1816

Gleadow A J W, Duddy I R, Green P F, et al. 1986. Confined fission track lengths in apatite: A diagnostic tool for thermal history analysis. Contrib Mineral Petrol, 94: 405–415

Green P F, Duddy I R, Gleadow A J W, et al. 1985. Fission track annealing in apatite: Track length measurements and the form of the Arrhenius plot. Nucl Tracks Radiat Meas, 10: 323–328

Guo Z J, Wu C D, Zhang Z C, et al. 2005. Mesozoic-Cenozoic relationships between Tianshan Mountain and peripheral basins: Evidence from sedimentology and exhumation of Jurassic in Houxia area, Urumqi (in Chinese). Geol J China Univ, 11: 558–567

Guo Z J, Zhang Z C, Wu C D, et al. 2006. The Mesozoic and Cenozoic exhumation history of Tianshan and comparative studies to the Junggar and Altai Mountains (in Chinese). Acta Geol Sin, 80: 1–15

Hendrix M S, Graham S A, Carroll A R, et al. 1992. Sedimentary record and climatic implications of recurrent deformation in the Tian Shan: Evidence from Mesozoic strata of the north Tarim, south Junggar, and Turpan basins, northwest China. Geol Soc Am Bull, 104: 53–79

Hendrix M S, Dumitru T A, Graham S A. 1994. Late Oligocene-early Miocene unroofing in the Chinese Tianshan: An early effect of the India-Asia collision. Geology, 22: 487–490

House M A, Wernicke B P, Farley K A. 1998. Dating topography of the Sierra Nevada, California, using apatite (U-Th)/He ages. Nature, 396: 66–69

Hurford A J, Green P F. 1983. The Zeta age calibration of fission-track dating. Chem Geol (Isotope Geoscience Section), 41: 285–317

Hurford A J, Hammerschmidt K. 1985. ^{40}Ar/^{39}Ar and K-Ar dating of the Bishop and Fish Canyon Tuffs: Calibration ages for fission-track dating standards. Chem Geol (Isotope Geoscience Section), 58: 23–32

Ketcham R A, Donelick R A, Carlson W D. 1999. Variability of apatite fission track annealing Kinetics III: Extrapolation to geological time scales. Am Mineral, 84: 1235–1255

Ketcham R A, Carter A, Donelick R A, et al. 2007. Improved modeling of fission-track annealing in apatite. Am Mineral, 92: 789–798

Ketcham R A. 2009. HeFTy version 1.6.7. Austin: University of Texas

Li L, Chen Z L, Qi W X, et al. 2008. Apatite fission track evidence fro uplifting-exhumation processes of mountains surrounding the Junggar basin (in Chinese). Acta Petrol Sin, 24: 1011–1020

Li J Y, Wang K Z, Li Y P, et al. 2006. Geomorphological features, crustal composition and geological evolution of the Tianshan Mountains (in Chinese). Geol Bull China, 25: 895–909

Ma Q, Shu L S, Zhu W B. 2006. Mesozoic-Cenozoic burial, uplift and exhumation: A profile along the Urumqi-Korla highway in the Tianshan Mountains (in Chinese). Xinjiang Geol, 24: 99–104

Métivier F, Gaudemer Y. 1997. Mass transfer between eastern Tien Shan and adjacent basins (central Asia): Constraints on regional tectonics. Geophys J Int, 128: 1–17

Najman Y, Pringle M, Godin L, et al. 2001. Dating of the oldest continental sediments from the Himalayan foreland basin. Nature, 410: 194–197

Reiners W P, Zhou Z Y, Ehlers T A, et al. 2003. Post-orogenic evolution of the Dabie Shan, eastern China, from (U-Th)/He and fission-track thermochronology. Am J Sci, 303: 489–518

Reiners W P, Brandon M T. 2006. Using thermochronology to understand orogenic erosion. Annu Rev Earth Planet Sci, 34: 419–466

Reiners P W, Nicolescu S. 2006. Measurement of parent nuclides for (U-Th)/He chronometry by solution sector ICP-MS, ARHDL Report 1. University of Arizona

Reiners P W. 2007. Thermochronologic approaches to Paleotopography. Rev Mineral Geochem, 66: 243–267

Shen C B, Mei L F, Liu L, et al. 2006. Evidence from apatite and zircon fission track analysis for Mesozoic-Cenozoic uplift thermal history of Bogda Mountain of Xinjiang, northwest China (in Chinese). Mar Geol Quat Geol, 26: 87–92

Shen C B, Mei L F, Zhang S W, et al. 2008. Fission-track dating evidence on space-time difference of Mesozoic-Cenozoic uplift of the Yilianhabierga Mountain and Bogda Mountain (in Chinese). J Mineral Petrol, 28: 63–70

Sobel E R, Dumitru T A. 1997. Thrusting and exhumation around the margins of the western Tarim Basin during the India-Asia collision. J Geophys Res, 102: 5043–5063

Shu L S, Wang B, Yang F, et al. 2003. Polyphase tectonic events and Mesozoic-Cenozoic basin-range coupling in the Chinese Tianshan belt. Acta Geol Sin, 77: 457–467

Shuster D W, Ehlers T A, Rusmore M E, et al. 2005. Rapid glacial erosion at 1.8 Ma revealed by $^{4}He/^{3}He$ thermochronometry. Science, 310: 1668–1670

Vermeesch P, Seward D, Latkoczy C, et al. 2007. Alpha-emitting mineral inclusions in apatite, their effect on (U-Th)/He ages, and how to reduce it. Geochim Cosmochim Acta, 71: 1737–1746

Wang W, Zhou Z Y. 2009. Reconstruction of palaeotopography from low-temperature thermochronological data. In: Lisker F, Ventura B, Glasmacher U A, eds. Thermochronological methods: From palaeotemperature constraints to landscape evolution models. Special Publication of Geological Society of London. (324): 99–110, doi: 10.1144/SP324.8

Wang X W, Wang X W, Ma Y S. 2007. Differential exhumation history of Bogda Mountain, Xinjiang, northwestern China since Late Mesozoic (in Chinese). Acta Geol Sin, 81: 1507–1517

Windley B F, Allen M B, Zhang C, et al. 1990. Paleozoic accretion and Cenozoic deformation of the Chinese Tien Shan Range, central Asia. Geology, 18: 128–131

Xu C H, Zhou Z Y, Van den Haute P, et al. 2005. Apatite fission track geochronology and its tectonic correlation in the Dabieshan orogen, Central China. Sci China Ser D-Earth Sci, 48: 506–520

Yang S F, Chen H L, Chen X G, et al. 2003. Cenozoic uplifting and unroofing of southern Tien Shan, China (in Chinese). J Nanjing Univ (Natural Sci), 39: 1–8

Yin A, Nie S, Craig P, et al. 1998. Late Cenozoic tectonic evolution of the southern Chinese Tian Shan. Tectonics, 17: 1–27

Zhang L C, Wu N Y. 1985. Geological structure and evolution of the Tianshan Mountains (in Chinese). Xinjiang Geol, 3: 1–13

Zhang P Z, Deng Q D, Yang X P, et al. 1996. Late Cenozoic tectonic deformation and mechanism along the Tianshan Mountain, Northwestern China (in Chinese). Earthq Res China, 12: 127–140

Zhang Z, Zhu W, Shu L, et al. 2009. Apatite fission track thermochronology of the Precambrian Aksu blueschist, NW China: Implications for thermo–tectonic evolution of the north Tarim basement. Gondwana Res, 16: 182–188

Zhang Z C, Guo Z J, Wu C D, et al. 2007. Thermal history of the Jurassic strata in the northern Tianshan and its geological significance, revealed by apatite fission-track and vitrinite-reflectance analysis (in Chinese). Acta Petrol Sin, 23: 1683–1695

Zhou Z Y, Xu C H, Reiners P W, et al. 2003. Late Cretaceous-Cenozoic exhumation of Tiantangzhai region of Dabieshan orogen: Constraints from (U-Th)/He and fission track analysis. Chin Sci Bull, 48: 1151–1156

Zhu W B, Shu L S, Wan J L, et al. 2006. Fission-track evidence for the exhumation history of Bogda-Harlik Mountains, Xinjiang since the Cretaceous (in Chinese). Acta Geol Sin, 80: 16–22